Electron precession: A guide for implementation

C. S. Own and L. D. Marks
Department of Materials Science and Engineering, Northwestern University, 2220 Campus Drive, Cook 2036, Evanston, Illinois 60208

Wharton Sinkler
UOP LLC, 25 East Algonquin Road, Des Plaines, Illinois 60017-5017

The design approach for electron precession systems designed at Northwestern University is described, and examples of systems retrofitted onto two different transmission electron microscopes using this method are demonstrated. The precession diffraction patterns from these instruments are of good quality while simultaneously being very easy to acquire. A 15-minute procedure for aligning these instruments is described in the appendix. Partnering this user-friendly and inexpensive hardware implementation with fast and user-friendly crystallography software offers potentially speedy and routine solution of crystal structures. © *2005 American Institute of Physics.* [DOI: 10.1063/1.1866612]

I. INTRODUCTION

The phase problem in crystallography has largely been solved for the case of x-ray radiation for many years. Structure determination is routine for both inorganic compounds and biological specimens using patterns acquired using synchrotron radiation or from laboratory instruments. However, as the length scale of structures of interest has decreased, the electron microscope has become increasingly important in the crystallography field. For many problems, it is the only available tool that can probe the scale of interest.

Probe sizes in recent aberration-corrected electron microscopes have bettered one Angstrom, and chemical and spatial information from single atoms in radiation resistant materials is readily acquired.[1–3] However, even with materials that damage under the electron beam, very precise information about the average structure can be gained from less sophisticated instruments through direct phasing of diffraction patterns.[4–6] The caveat with these conventional machines is that current methods require much guesswork and analysis to find the true structure. Electrons are scattered by matter about 1000 times more strongly than x rays; consequently dynamical scattering causes intensities to deviate from the square of structure factor amplitude. Additionally, multiple scattering events give rise to forbidden reflections not present in the single-scattering (kinematical) case. Except for instances of extremely thin specimens, surface structures, or for weakly scattering materials, direct methods techniques often do not provide a straightforwardly interpretable solution.

The electron precession technique is a promising recent innovation in electron crystallography.[7] Rather than using dynamical data with the kinematical computer codes widely available, precession attempts to make the data more kinematical and therefore more amenable to simple crystallographic phasing techniques. Recent analyses show that direct methods performed on precession data from heavy metal oxides, characteristically strongly dynamical-scattering structures, consistently yield well-defined potential maps that clearly identify cations in the structure.[8] The advantage of the precession technique is that with some processing the experimental precession data appear to be ordered similarly enough to kinematical intensities to provide the solution—or something very close to the solution—quite readily via direct methods with minimal user intervention.

An obstacle to wider use of any new technique is inherent scarcity of equipment on which to conduct studies. Past reports using precession have described experiments and compared precession to conventional methods, but only cursory information has been given about implementation of the precession devices used.[7,9–12] Additionally, these investigations have not described experiment parameters in detail. It is now apparent that experiment geometry is critical to the behavior of the resulting dataset,[8,13] thus a comprehensive set of variables including cone semiangle, convergence, probe size, and specimen image stability should necessarily accompany such studies. This paper provides a straightforward do-it-yourself scheme for retrofitting precession capability onto a conventional transmission electron microscope, and concurrently provides a common language for describing precession experiments. Two example implementations on older instruments are provided, with attention paid to technical specifics.

II. BACKGROUND

The Vincent–Midgley technique originally stemmed from studies conducted using measurements of high-order reflections in CBED patterns from an Al–Ge crystalline phase.[14] Higher-order reflections were found to be more kinematical and were useful in aiding kinematical refinements of inorganic nanocrystals. The precession scheme is a logical extension of this; it exploits the diminished dynamical effects of the off-zone condition by using a hollow cone of illumination obtained through fast serial tilt deflections above the specimen. A consequent de-tilt of diffracted beams below the
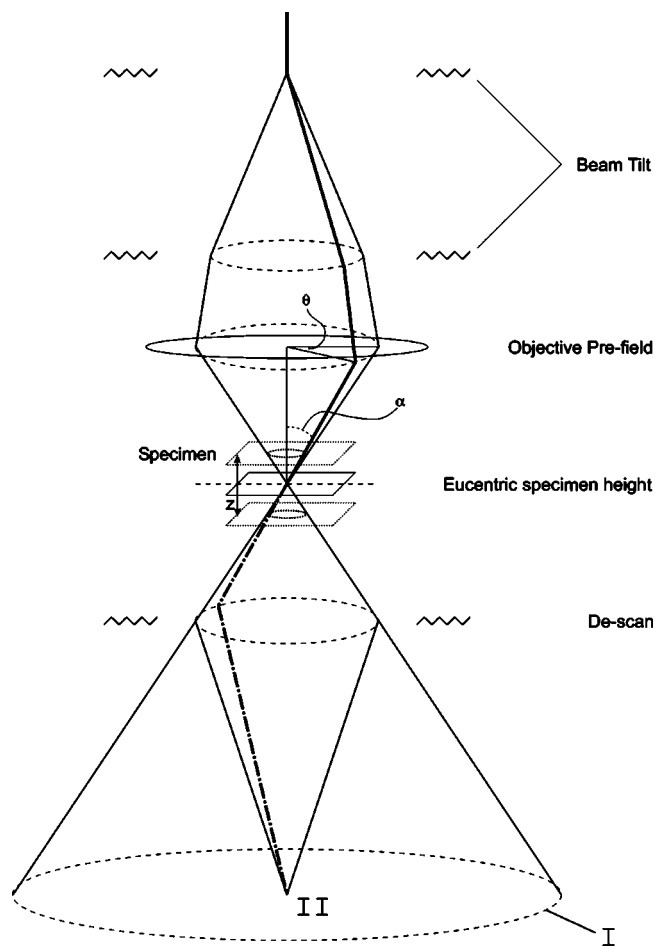
FIG. 1. Precession geometry in a modern condenser-objective TEM with double deflection coil system showing the path of the precessed transmitted beam. The objective prefield acts as an additional condenser lens. Circle I is generated by the beam tilt scan. De-scan collapses circle I down to point II.

specimen is necessary to restore the conically rocked beams to points in diffraction space. This performs an inherent integration over the series of tilt conditions and generates a directly interpretable pseudo-kinematical zone axis pattern.

In this paper the tilt above the specimen will be referred to as BT (beam tilt) and the complementary tilt below the specimen will be called DS (de-scan). Precession electron diffraction patterns will be called "precessed DP's" and conventional selected-area or focused-probe diffraction patterns will simply be called "DP's."

Figure 1 is a cartoon of a modern condenser-objective instrument showing the ray paths traversed by a precessed transmitted beam. In reciprocal space, the BT operation is equivalent to rocking the Ewald sphere about a pivot point corresponding to the forward-scattered reflection (origin) of the zeroth-order Laue zone (ZOLZ). The sphere intersects each reflection in reciprocal space throughout a range of excitation errors while spending very little time dwelling in the on-zone condition where dynamical effects are most prominent. A theoretical description based on the two-beam condition has been proposed by Vincent and Midgley and by Gjønnes.[7,15]

For practical implementation of precession the key requirements are:

(1) The precessed incident beam must yield a circular cone of directions about the crystal zone axis.
(2) The de-scan must bring the diffracted beams together to form uniform points (or nonoverlapping disks in the case of beam convergence) for accurate measurement.
(3) If spatial accuracy is desired in the experiment (e.g., fine-grained polycrystalline specimens), the conical probe fulcrum must intersect the specimen precisely in three-dimensional space.

Review of previously reported instruments: The earliest precession instrument was by Vincent and Midgley in 1994 based on a Philips EM430 operating at 300 kV.[7] A Wien bridge oscillator provided the precession scan signals; frequency was capped at 30 Hz to prevent distortions due to deflector bandwidth limitations. The stock instrument included inputs for beam tilt, however the de-scan circuitry did not support external control thus the de-scan controls were completely replaced by the analog oscillator. While this instrument was reported to yield better than a 10 nm diameter probe in convergent illumination mode in theory, the implementation was limited to a 100 nm area due to probe-wandering caused by aberrations. The tilt range was reported at 8° (~140 mrad), however the earliest experiments were conducted below 25 mrad and later experiments on Al_mFe using more parallel illumination had a 40 mrad semiangle, both consistent with the <50 mrad figure typical for this type of optical distortion-limited system. Projector lens distortion was the primary limiting factor which caused gross errors in the de-scan at moderate angles and complicated automated measurement.

Patterns from the Al_mFe study were measured by digitizing the negative on a light box using a CCD, then integrating the line profile through each spot after background removal.[16] Line profiling assumes each reflection exhibits perfect circular symmetry, which is acceptable for the convergent beam case since spatial constraints on the film are relaxed; for (near-)parallel illumination, the constraints are much tighter. Convergent mode precession limits measurable patterns to sparse diffraction patterns, making surfaces and superstructures more difficult to study.

Gemmi has developed a precession instrument on a 300 kV Philips CM30T chassis that operates at 35 Hz.[17] The microscope CPU can generate appropriate scan signals for hollow cone parallel illumination conditions in the selected area channeling pattern operating mode. The scan signals are supplied to the external inputs of the microscope, which digitizes them and outputs appropriate currents to the deflector arrays. One of the limitations of this type of system is that signal quality at the coils is limited by sampling rate and precision of the A-to-D converters at the input and later by the D-to-A's supplying the coil drivers. Due to this, some difficulty with de-scan precision in early revisions were reported that appear to have later been resolved. The structure of Ti_2P was solved using a three-dimensional dataset merged from several zone axis patterns collected on the precession-enabled CM30T, showing successful use of precession intensities in structure solution where SAED data had proven insufficient.[11] The device was operated with parallel illumi-
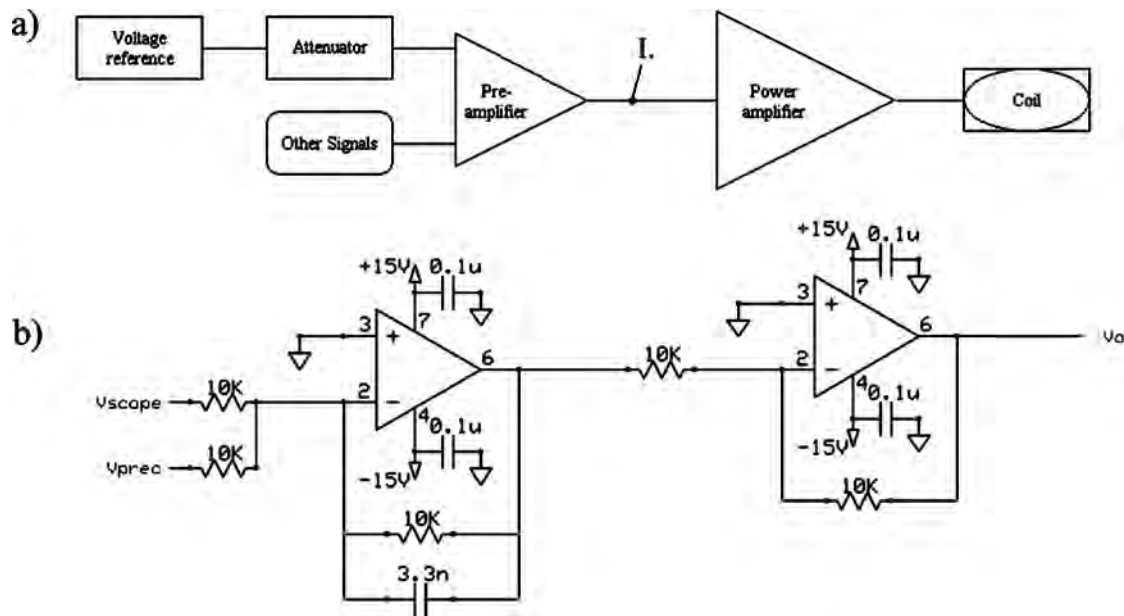
FIG. 2. (a) Generic dc amplifier for driving an electromagnetic coil. (b) Mixer-buffer circuit used to add precession capabilities to a deflector amplifier. The first stage mixes the normal microscope signal with that from the precession and is followed by an inverting buffer stage that corrects phase and isolates the mixer from downstream components. This circuit can be installed at point I in (a).

nation, forming sharp spots and a moderate tilt angle of 17 mrad was reported, limited by distortions in the optics.

The utility of these two instruments show the technique's potential as a crystallography tool, however, optical distortions clearly limited both instruments' performance. The following examples demonstrate an approach using simple geometric distortion compensations to improve precession quality. In the first example, the corrections were essential but proved to be insufficient for high-precision precession due to instrument limitations. Better design and careful refinement of alignment procedure yielded very good performance and high reliability for the second system described.

III. DESIGN APPROACH

Beam deflection above the specimen with complementary de-scan below can be produced in most modern instruments using the beam tilt coils and the projector image shifts by supplying appropriate scan signals directly to the analog coil driver circuits. We aimed to provide a simple and straightforward human-machine interface to control precession hardware designed for stability and reliability within the framework of the existing system without affecting original functionality.

A. Stock instrument hardware

Deflection systems inside common TEMs follow a general theme wherein a control voltage is supplied to a current amplifier which drives current in a coil [Fig. 2(a)]. In such systems, control voltages are typically under 10 V, and currents in the coils do not exceed a couple of amperes. Since microscopes are used primarily for steady-state operation (scanning microscopes excluded), coil drivers in many microscopes have been designed for dc operation and stability and thus do not have the bandwidth to support precession. A

simple coil driver stage based on power operational amplifiers is provided later in this paper to demonstrate a solution.

Most deflection coils are dipoles, meaning two windings are used to deflect the beam in orthogonal directions within a plane perpendicular to the optic axis. Identification of the axes in each coil is key since rotations or opposing field polarities often exist between deflectors throughout the column; this knowledge will prevent mismatch of precession direction between scan and de-scan and give an idea of the phase shift between the coil sets that will be applied during alignment.

B. Circuit modifications

The precession signal can be conveniently inserted at any point in the circuit where the signal is in voltage form and low in amplitude (a few volts). An example is between the pre- and power amplifer at point I in Fig. 2(a), where a small amplifier module can be inserted in series to combine the scan signal with microscope console commands. Simple circuit building blocks based on operational amplifiers (op-amps) are very suitable for this purpose, being easy to use due to compact and simple physical circuit layout and high intrinsic power supply rejection ratio (e.g., a variety of supplies can be used, including unregulated types).

For advanced op-amp usage details, the reader is referred to an analog circuits textbook or IC application notes.[18–20] A diagram of a common operational amplifier, the LM741, in the DIP8 package is depicted in Fig. 3(a). It possesses two signal inputs (inverting and noninverting), output, power supply inputs, and pins for offset nulling. Figures 3(b)–3(d) show the most basic configurations for amplification using this type of device. The noninverting amplifier outputs a signal with the same polarity as the input waveform whereas the inverting amp naturally inverts polarity of the input. The gain of each configuration, shown to the right
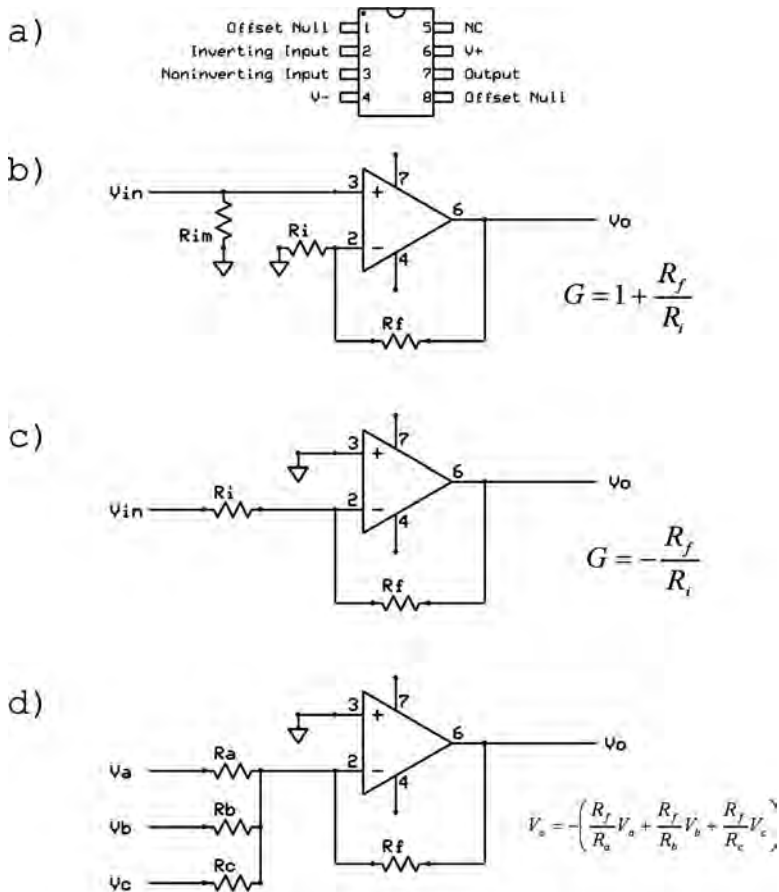
FIG. 3. (a) LM741 op-amp, DIP8 package. (b) Noninverting, (c) inverting, and (d) mixer (inverting) operational amplifier circuits.

of each circuit, is set by a combination of the feedback resistor R_f and a second resistor R_i. For precession, two inputs are necessary, one for steady-state control from the microscope console and the other for the oscillatory scan signal. In certain cases where the zero-point is significant (e.g., an "inputs-are-zeroed" indicator trigger), the amplifier may require offset trimming to remove voltage offset at the output. Some devices available on the market feature low intrinsic offset voltage to address this without user intervention.

While it is possible to convert op-amps within the stock circuits into mixers, we chose to use add-on mixer modules placed in series on low-level signal lines for versatility. Figure 2(b) shows the mixer-buffer module used in both implementations described in this paper, comprising a single-ended inverting mixing amplifier followed by an inverting buffer stage that corrects polarity and isolates the summer from downstream electronics. One amplifier circuit is used for each input (four total). A 15 V split supply was used, and appropriate bypassing was used to enhance supply performance. The 3.3 nF feedback capacitor in the mixer stage (optional) limits the bandwidth to about 5 KHz in the case that downstream components are sensitive to the high-frequency components from the signal generator's nonoversampling DAC. A low-distortion part (e.g., film-type) is preferred for this feedback capacitor. Basic constraints for selecting a specific amplifier device off the shelf are: high input impedance, moderate bandwidth, high power supply rejection ratio, and unity gain stability for the output buffer (second gain stage). FET-input (field-effect transistor) based

operational amplifiers that operate at unity gain in a moderate frequency range of dc to a few hundred kHz are quite suitable.

While operational amplifiers in general have excellent supply noise rejection, a well-designed power supply is nevertheless critical for performance. A split voltage supply is required for amplifying bipolar signals. The supply voltage rails should exceed the maximum signal amplitude by a fair margin to account for dropout voltage for the active devices, additionally it should be noted that many small-signal op-amps perform best when powered near maximum rated supply voltage. Supplies of ±15 V are common in microscopes and it is often sufficient to use the onboard supply (commonly accessible from test points on the signal board). Alternatively, an external supply can be used to power the amplifier so that the supply is immune to fluctuations caused by circuits elsewhere in the microscope and vice versa.

It is relevant to note that while beam tilt is controlled by two inputs at the console, 4 or 6 independent windings in a stacked coil pair work in combination to provide the tilts. Many microscopes allow high-level beam tilt control from just two analog signals because shift-tilt alignment has traditionally been executed in analog circuitry; the precession scheme presented here applies to this type of microscope. Modern digital microscopes now more commonly accomplish shift-tilt alignment in the digital domain, hence two scan signals would be insufficient, requiring low-level modification of individual coil drivers (e.g., extra scan inputs) and additional programming to accomplish conical illumination.

C. PC hardware

A PCI-671x series board by National Instruments was chosen for the Northwestern systems. This board employs 12-bit DACs (ample resolution for precession) to generate signals in the range of ±10 V. Its main strength is on-board cyclic buffering which allows a fast non-CPU-limited output rate. Target operation rate is 60 cycles per second with an angular resolution of at least 360 individual tilt points; for four channels, this is under 100 000 combined samples per second and well within the 1 MS/s limit for this board. Acquisition and control boards from other vendors may be equally suitable and can offer higher performance.

A primary concern with PC-based systems is inherently dirty ground due to switching power supplies and digital circuitry. In general, the PC's ground reference should be bridged to the microscope near the relevant signal circuitry but placed at a common point that offers stiff earthing. Additionally, long runs of cable should be shielded to prevent fields from modulating the signal. To prevent ground loops, the shield should be connected to ground only at one end of the interconnections (preferably at the source). For microscopes that require very high stabilities, differential scan signals should be utilized.

D. Software

The scan generator provides four computer-generated sinusoidal signals calculated by a software routine. Deflection coordinates for each point in the conical scan are calculated, sent to the hardware buffer, and the subsequent waveforms are outputted 90° out of phase to describe a circle of deflection points where the phase difference polarity defines the direction of rotation in each deflector plane. Aberrations in the objective lens can be compensated by adjusting deflection coordinates in the BT scan to counteract the effect of the aberration contours in the lens. The DS coil deflections are applied in the opposite direction of the tilt to bring the circle generated by BT scan down to a point in the diffraction plane (point II vs circle I in Fig. 1). The DS is phase shifted with respect to the BT scan by a fixed value ϕ.

The DS controls can be used to circumvent distortions in the projector deflectors and lens, or to remove the effect of small residual aberrations not eliminated by the BT. With care the integrated intensities can be brought down to measurable spots a fraction of a milliradian in diameter. Small errors in BT can be readily compensated by careful de-scan alignment even when moderate to high cone semiangles are used ($\alpha > 25$ mrad).

While astigmatism in magnetic lenses is described by hyperbolic functions, approximate twofold and threefold functions are sufficient for their compensation. The software algorithms that generate these compensations are based on the following set of relations:

$$x_1 = A_1 \cdot \cos \theta,$$

$$y_1 = A_1 \cdot \sin \theta,$$

$$x_2 = s \cdot \cos \theta,$$

$$y_2 = -s \cdot \sin \theta,$$

$$x_3 = [A_3 \cdot \cos(3 \cdot (\theta + \phi_3))] \cdot \cos \theta,$$

$$y_3 = [A_3 \cdot \cos(3 \cdot (\theta + \phi_3))] \cdot \sin \theta,$$

$$x_{out} = [(x_1 + x_2) \cdot \cos \phi_2 + (y_1 + y_2) \cdot \sin \phi_2] + x_3,$$

$$y_{out} = [-(x_1 + x_2) \cdot \sin \phi_2 + (y_1 + y_2) \cdot \cos \phi_2] + y_3.$$

The functions x_1 and y_1 represent the basic oscillatory functions that produce the precessed circle as θ traverses 2π radians. Functions x_2, y_2, x_3, and y_3 are used to generate two- and threefold compensations, where the variable s is a scaling factor for the twofold elliptical function related to the base deflection amplitude (cone semiangle α), and ϕ_2 and ϕ_3 are phase shifts that rotate these two- and threefold compensation functions. These constituents yield the functions x_{out} and y_{out}, which contain various prefield correction amplitudes in addition to the conical precession scan. In practice, the correction magnitude is on the order of 1% of the base deflection amplitude.

The software interface comprises scan amplitude controls, the twofold and threefold compensations described above, and phase shift ϕ between BT and DS scans. Additionally, the software allows precession rate control and precise tuning of frequency and angular resolution. The interface, based on LabView visual language, is available for download.[21]

Lens distortions in the lower column can complicate intensity quantification at higher α. For large cone angles, the quality of precessed diffraction spots decreases with increasing cone angle and diffraction spot centers become displaced in the diffraction plane due to projector distortions [Fig. 10(a)]. This was a problem on the CM30T on which the first precession instrument was based. For some microscopes, the maximum possible tilt may be restricted by objective lens aberrations before postspecimen distortions become a limiting factor.

The key aim for this design approach has been to balance function, usability, and complexity. Through graphical-tool-based object-oriented software to control digital electronics, the system preserves the intuitive analog feel of stock instrument yet is not limited by the inflexibility and inherent design complexity of a fully analog system. With distortion compensation, the precession pattern quality improves dramatically, and images can be digitized readily by automated cross-correlation methods, such as those in Electron Direct Methods.[22]

The following example systems show that retrofit of precession mode onto conventional instruments is not difficult, and (perhaps more importantly) that a good-performance implementation can be very inexpensive. The systems described each required less than US$2000 in parts costs. Excellent results can be expected if the most important requirements are met, namely compensation of aberrations, eucentric height correction, and careful user alignment. As more microscopes are being fitted with advanced capabilities
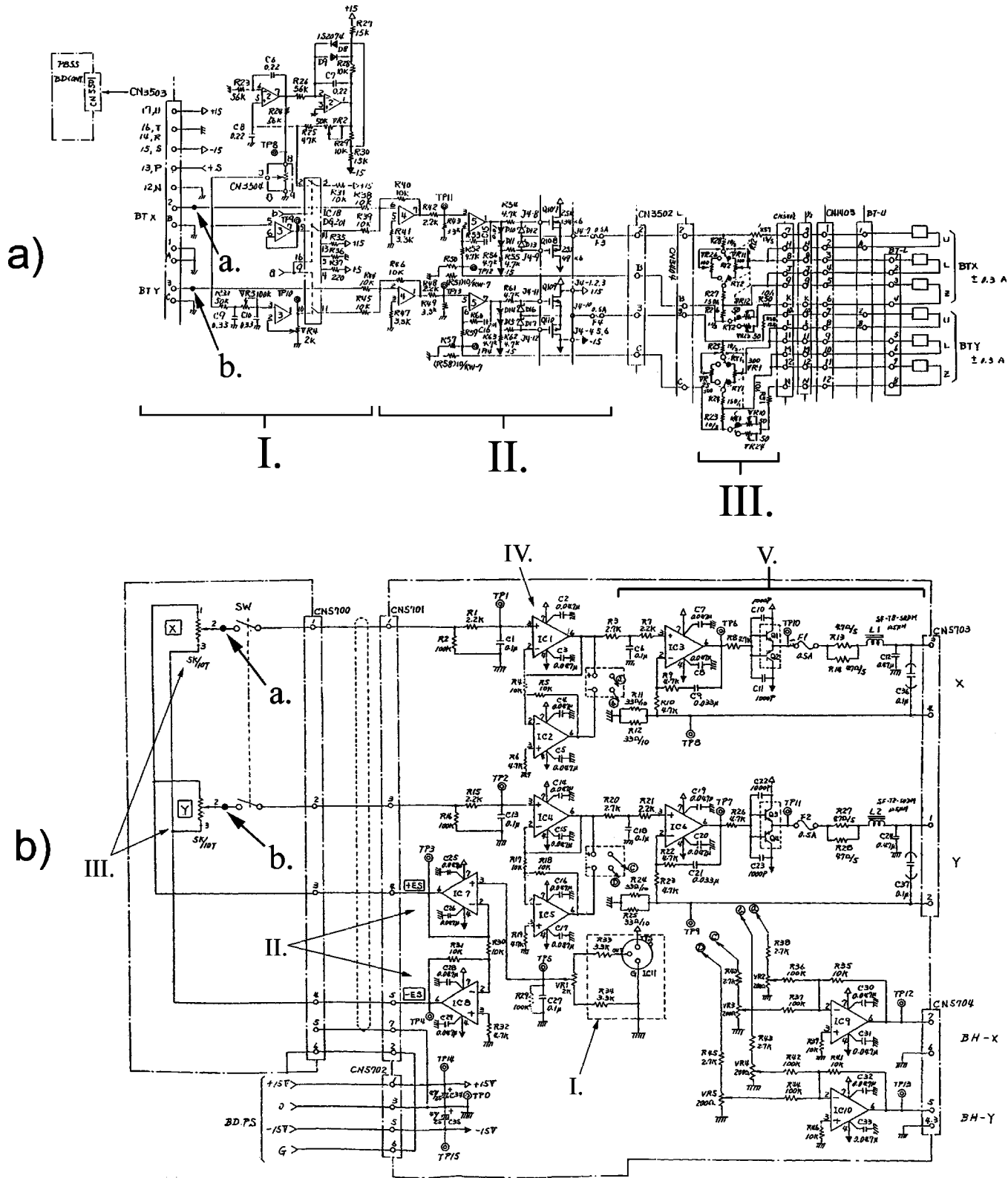
FIG. 4. (a) *BD STB* circuit schematic. (b) *Image S.* circuit schematic. Courtesy Hitachi High Technologies Corp.

such as hollow cone illumination and STEM mode, precession performance should steadily increase accompanied by ease of installation. Many new instruments support external control inputs, which—provided that suitable bandwidth is available—will simplify the requirements for custom hardware retrofit for future precession instruments.

IV. EXAMPLES

A. Example 1: Hitachi H-9000

The Hitachi UHV H-9000 is a 300 kV instrument designed for high resolution imaging and for diffraction. The instrument incorporates a special SA imaging mode for se-
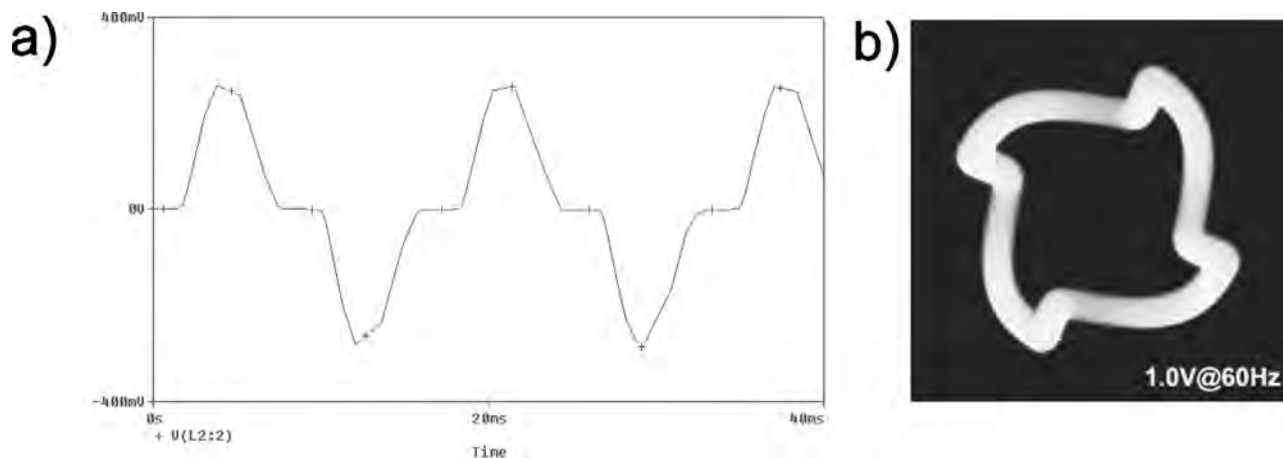
FIG. 5. (a) Simulated waveform for the H-9000 bipolar push–pull DS amplifier demonstrating crossover distortion. At each zero-crossing point, there is a plateau in the waveform. (b) A precessed beam tilt pattern demonstrates how this distortion manifests in the pattern: since x and y coils are out of phase by 90° a pinwheel pattern is generated.

lected area diffraction experiments intended to minimize SA errors. Because the system has a small objective polepiece gap, the stage allows only about ±10° tilt and the UHV side insertion system has been designed without eucentric height adjustment for mechanical simplicity.

A stacked pair of coils (a dipole and quadrupole) located several centimeters above the objective polepiece gap provides BT deflections and DS deflections are provided by a dipole deflector nested inside the projector lens. Upper column electronics can be found on the board *BD STB* under the left console and image shift is controlled from a small potentiometer box that controls an amplifier board mounted to the left console side, called *Image S.* The relevant section of the *BD STB* schematic is shown in Fig. 4(a). Each beam tilt axis is set using a digital encoder that controls a DAC (not shown) followed by a small unity gain buffer. This signal is in the range of ±5 V and supplies the BTX and BTY inputs on connector CN3503. Section I in the figure is part of an analog hollow cone driver called *STIG MON* for monitoring astigmatism in the objective lens (not active during normal operation). Following is the tilt amplifier (II) comprising an op-amp in summing mode driving a FET-output voltage-to-current amplifier. There is some biasing circuitry in this stage that ensures bandwidth for the tilt wobbler adjustment, favorable for precession because it offers operation up to about 1 kHz. Section III is a voltage divider and switching array used to split the current between the three coil windings for each tilt axis. Four user-accessible potentiometers in this stage control the division of current to each winding: these are the X_{main}, X_{vert}, Y_{main}, and Y_{vert} controls used during shift-tilt purity alignment.

The custom modules were retrofitted at points *a* and *b* in series with the input CN3503. The modules were built around an LM324 IC in DIP14 package (a quad 741 IC with class AB biasing). The BT mixer module was mounted onto a short length of 34-conductor ribbon cable that also serves as a quick-release pass-through extender for connector CN3503. Conductors 3 and 5 on the cable, corresponding to pins 2 and 3 of CN3503, were used to insert *X* and *Y* signals, respectively, and conductor 1 was used for the ground refer-

ence. Power was supplied to the add-on boards via the ±15 V supply pins on the *BD STB* and *Image S.* boards.

The image shift circuit is intended for steady state operation and is correspondingly quite different from BT [Fig. 4(b)]. The signal originates from a 10 V precision reference (I.), converted into ±4 V reference legs (II.) by an op-amp stage. These are divided into control voltages by linear potentiometers (III.) followed by a differential op-amp buffer stage (IV.) that feeds the coil amplifier (V.). The inverted leg of the differential buffer (not connected in this instrument) provides an optional compensation signal for an extra dipole deflector (BH-X, Y) earlier along the optic path. The DS current amplifier terminates in a bipolar push–pull output stage that delivers larger currents than the BT, around several hundred milliamps, to achieve appreciable deflections of the image on the viewing screen. The circuit is precise and has low noise for image stability.

While excellent for dc signals, the stock image shift circuit was found to be unsuitable for precession due to the class B problem. Push–pull amplification stages, if not properly biased, can cause distortion at the zero-crossing point of rapidly varying signals because each device in the complementary pair has a finite switching time (Fig. 5). A possible solution is to bias the output stage into class A to remove the distortion, however, working around the design proved difficult and the final solution took the form of a completely redesigned board based on power op-amps shown in Fig. 6 (see Ref. 13). This preserves the service warranty for the instrument and provides extra performance headroom. The *Image S.* circuit is broken at R3/R20 and the output of the preceding driver stage is routed directly to the custom DS amplifier board, bypassing the stock amplifier. The replacement amplifier consists of an OPA544T power operational amplifier in a current-sense feedback loop similar to that used in the stock circuit. Power and ground are supplied from *Image S.* and additional supply filtering is employed. The replacement unit extends usable bandwidth beyond 2 kHz.

Performance and limitations: The precession mode is typically operated at about 60 Hz to ensure ample intensity
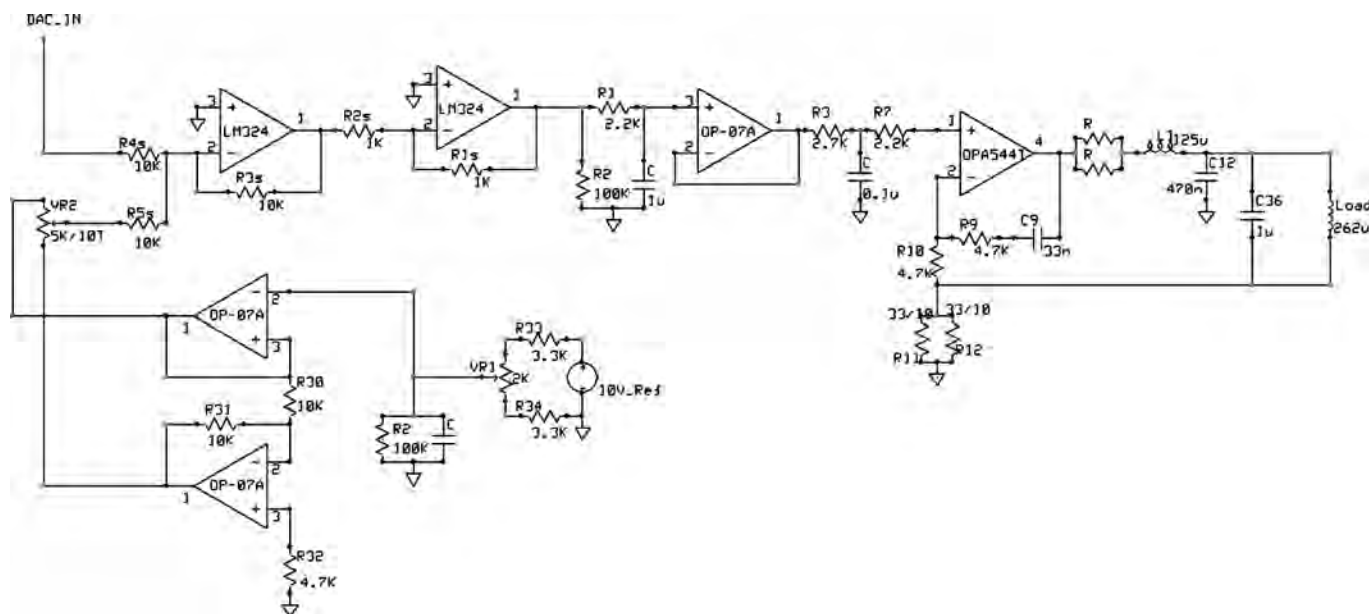
FIG. 6. Redesigned projector deflector circuit for the H-9000 (one channel only), incorporating the plug-in module for applying de-scan and higher bandwidth output amplifier.

averaging for short exposures. During operation, an artifact often appears in the scan due to power supply ripple identified by a "snail" (small kink in the circle pattern) that travels slowly around the BT circle. Its speed depends on the relation between the scan and mains frequencies. The artifact can be removed by precisely matching the scan rate with the oscillation frequency of the mains (can vary throughout the day, depending on the mood at the power company). On-site, the mains frequency typically varies between about 59.25 Hz to 60.25 Hz and can change during a microscopy session.

The H-9000-based precession instrument is limited by its lack of eucentric height adjustment and small tilt range ($\pm 10°$). Depending upon insertion conditions, the specimen height may deviate from optimum crossover by over 100 μm, limiting the spatial resolution of the precession probe. The shift-tilt purity correction range is insufficient to localize the probe. To circumvent this problem, precession is typically operated with selected area (SA) mode using parallel illumination: the SA aperture limits probe wandering by ensuring even illumination of the specimen. However, the probe size becomes limited by aperture size, and SA errors give rise to excess delocalization of illumination that cannot avoided because optimum lens excitation and specimen height are unavailable. Poor probe localization is the ultimate limitation of this system making nanocrystal precession diffraction studies difficult. The instrument nevertheless acquired patterns from large regions and isolated small particles rather well, giving good averaged patterns from sample regions about 200 nm in diameter. Measurable patterns have been acquired from $Mg_3V_2O_8$ and $La_4Cu_3MoO_{12}$ with this machine.[12] For the $La_4Cu_3MoO_{12}$ experiments, the cone angle of 25 mrad was large for this instrument and the spots became ill-defined and difficult to measure. Rather than employing the more accurate method of cross-correlation using average unitary spot motif (requires similar-shaped spots),

the intensities from this pattern were integrated after background subtraction from small masked regions around each spot.

B. Example 2: JEOL 2000FX

A second-generation precession instrument was constructed based on the JEOL 2000FX chassis located at UOP, LLC in Des Plaines, IL. The 2000FX is an analytical instrument well suited for precession since the polepiece supports high tilts by virtue of a well-developed convergent beam mode. The instrument included a $\pm 45°$ side-entry double-tilt holder and a model US1000 $2K \times 2K$ CCD camera from GATAN. This implementation drew upon the knowledge gained from the previous precession implementation and integrated some refinements that improved performance dramatically:

(1) Specimen holder *z*-height adjustment;
(2) Polepiece supports large tilts;
(3) Large CCD streamlines dataset acquisition. Beam blanking above specimen decreases radiation damage;
(4) Miniaturized plug-in modules using surface mount devices;
(5) Independent power supply (external);
(6) Improved grounding scheme;
(7) Updated software;

The 2000FX deflector electronics are located on a single board *DEF UNIT*, which controls all deflector coils in the column (accessible below the right-hand console behind an acrylic cover). The current values for each coil set, controlled by a pair of digital encoders, is stored in memory and held constant by the microscope computer, changing only when console control is passed to that coil set. The power amplifier design is common to most of the deflectors in the instrument and is simply replicated in each coil driver circuit
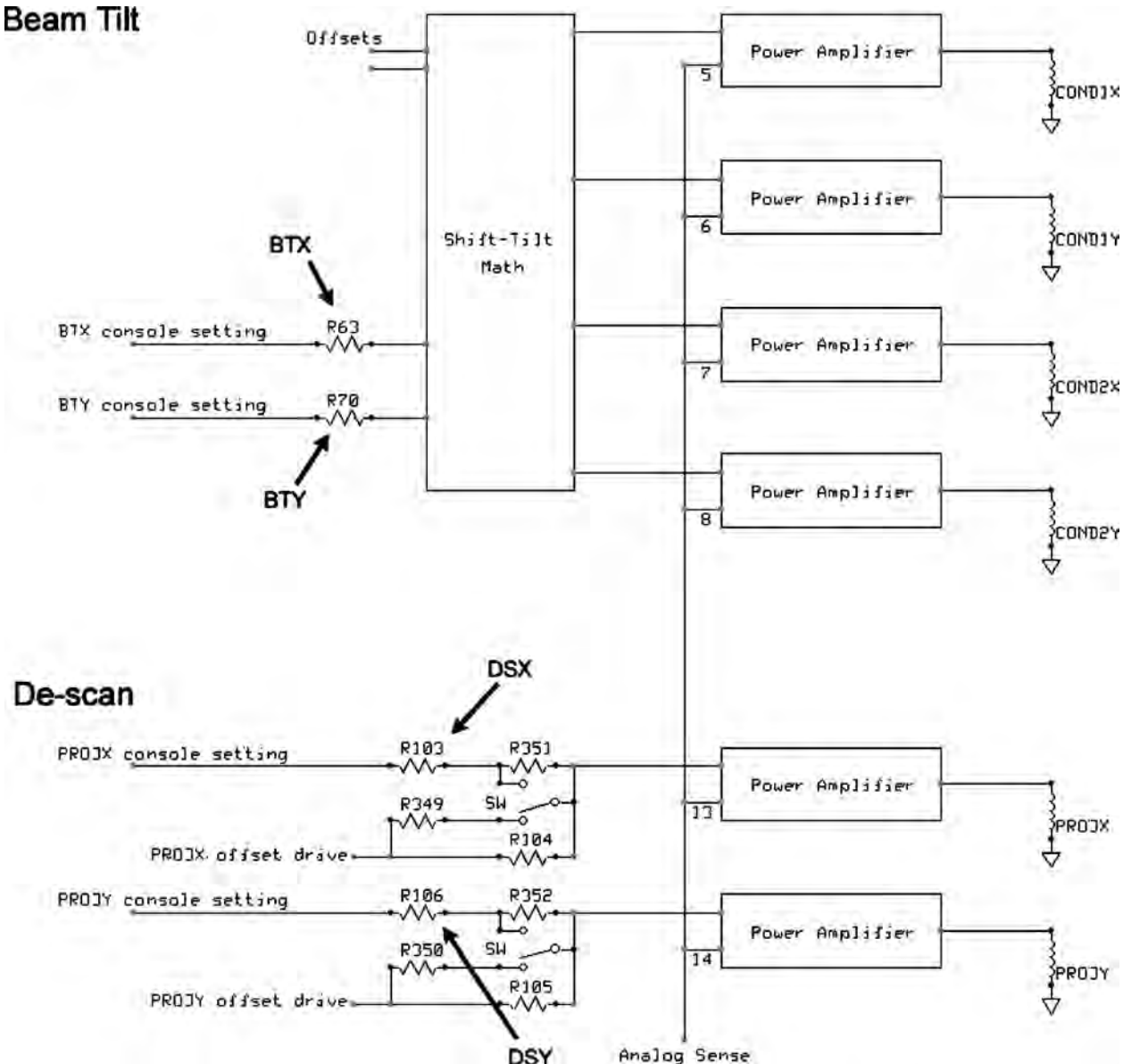
FIG. 7. *DEF UNIT* block diagram for JEOL 2000FX. (a) The schematic relevant for BT; (b) for DS. Points *a* and *b* in both figures are locations where the plug-in module should be inserted.

down the column. The 2000FX has provisions for a hollow cone illumination option, thus its deflectors can process fast scan signals without modification.

Block diagrams for the BT and DS amplifiers are shown in Fig. 7. Coils COND1,2X,Y provide BT deflections, and PROJX,Y denote the DS deflectors. For precession, the location at which the digital stage feeds the analog stage is an ideal location to insert the scan signal. The mixer modules can simply be inserted in series before resistors R63, R70, R103, and R106, corresponding to BTX, BTY, DSX, and DSY.

The plug-in modules [Fig. 8(a)] were based on Burr-Brown OPA2604 dual operational amplifiers in the SOIC8 package, low noise amplifiers designed for audio. Most of the electronics were migrated to surface mount easing installation by virtue of miniaturization. A simple dedicated linear regulated supply, comprising capacitive decoupling between two regulation stages, was built for the plug-in modules [Fig.

8(b)]. JEOL specifies <10 mV ripple for the *DEF UNIT*, which the custom supply meets. The supply and a National Instruments signal distribution board were incorporated into a project box that included BT and DS on/off toggle switches on the front panel for manual control independent of software. The PC DAC board interfaces with the project box via a 68-pin high-density cable, upper and lower coil outputs on the rear panel incorporate power leads and signal lines (isolated from each other via foil shields) into a single cable bundle for each module, and an additional terminal for the microscope ground is also provided. The ground connection from the microscope is shorted to the PC ground and can be broken with a toggle switch when precession is not used.

Performance and limitations: The instrument is operated with smallest condenser aperture for small probe, coherence, and low dose to protect the CCD. BT on the 2000FX can be operated in either a bright mode or dark mode; in the latter the control input is multiplied by a factor of 10 to increase
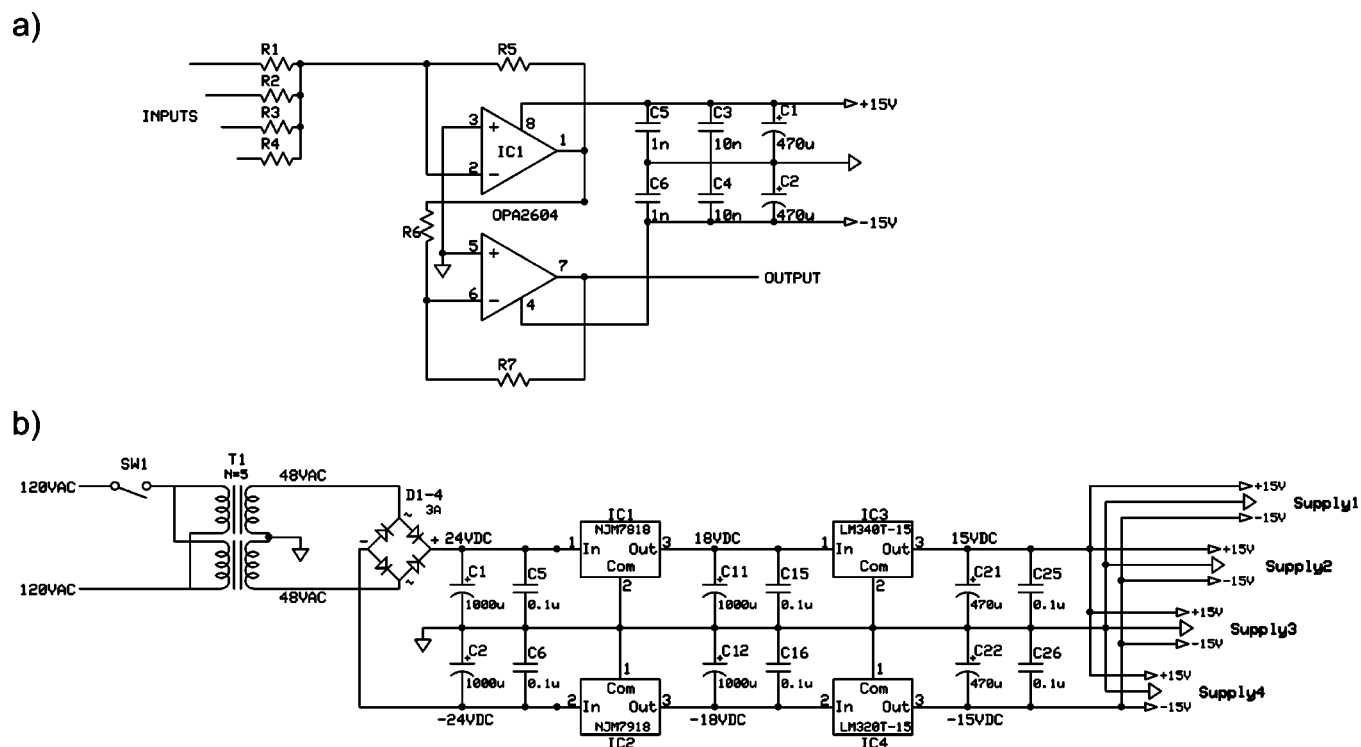
FIG. 8. Schematics for the 2000FX precession modification. (a) Schematic for plug-in module; (b) external power supply schematic.
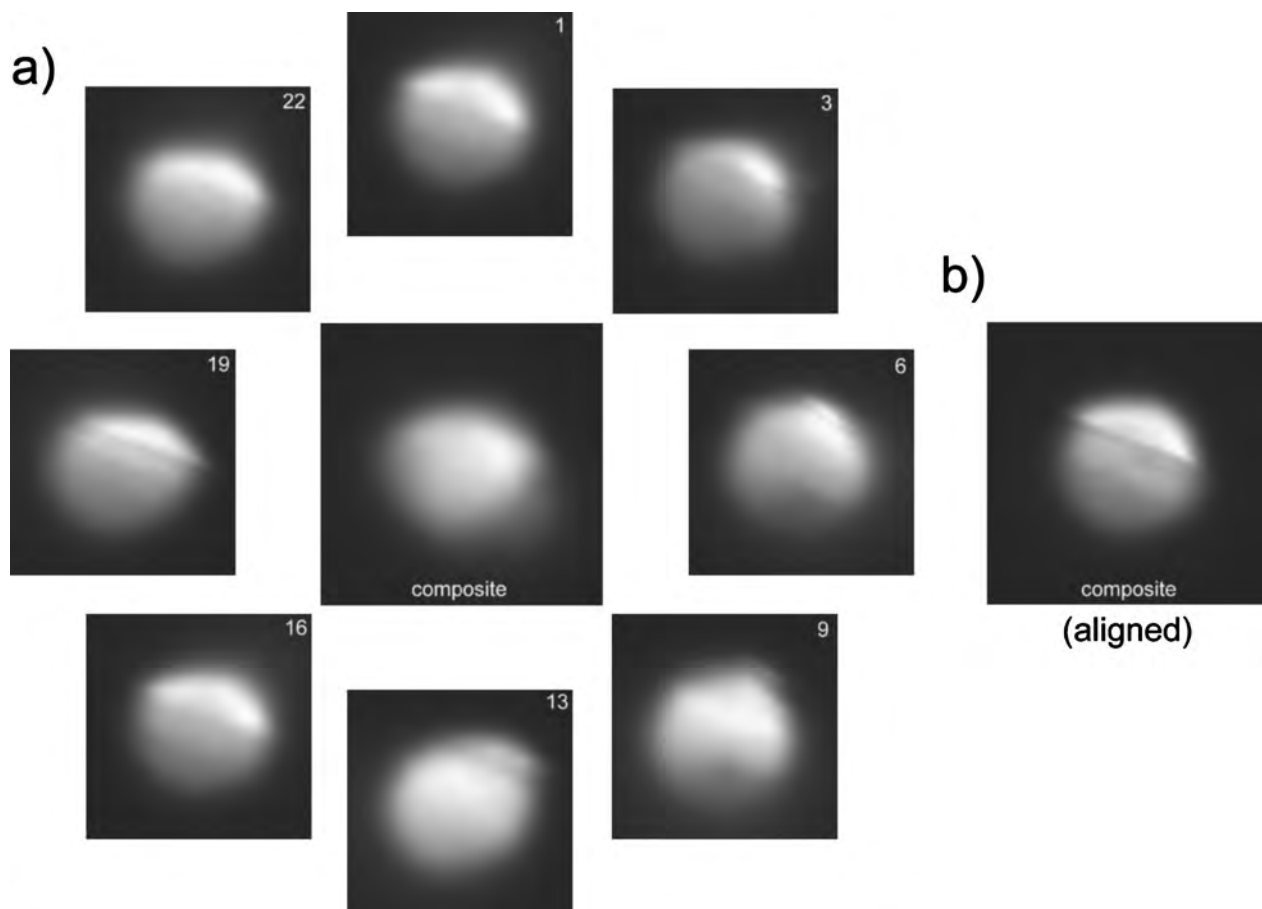

FIG. 9. (a) Montage of probe images during a revolution (close to aligned). 24 frames denote a full revolution; 8 of the 24 are shown here. The center image shows the composite of all tilts. Both probe and specimen image wander for unaligned condition, contributing to a blurry composite image. The right image (b) shows a well-defined specimen image and excellent alignment of cone pivot point after alignment. Probe size is about 50 nm.
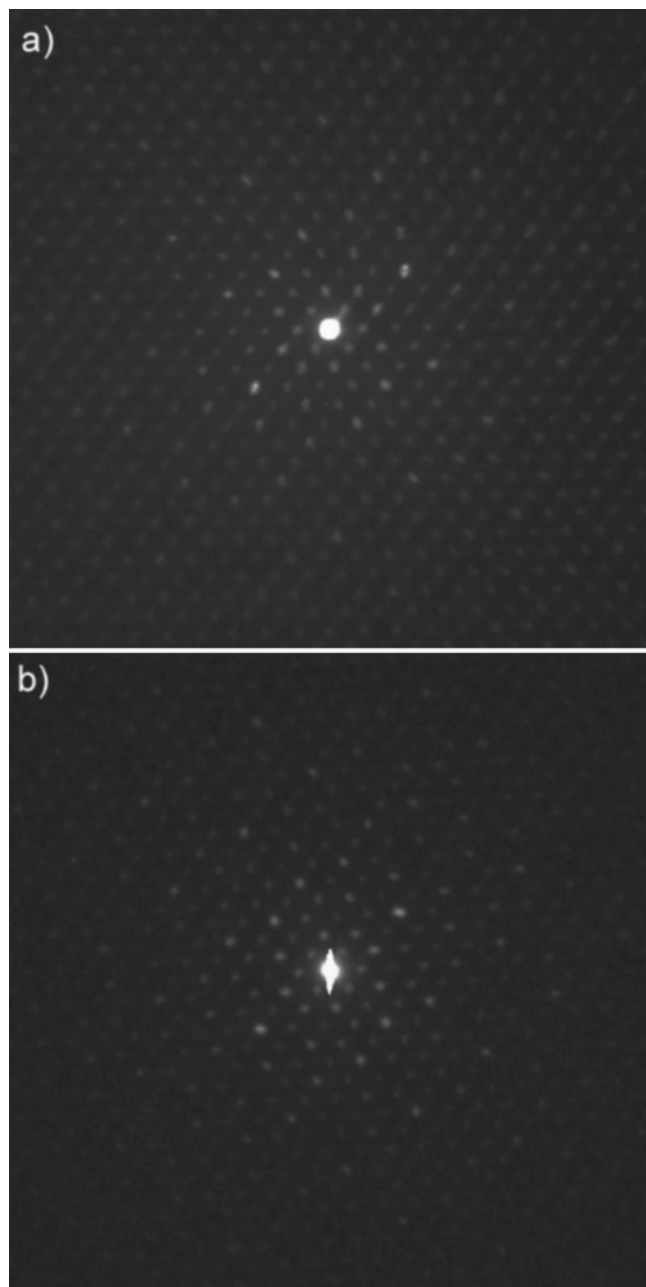
FIG. 10. Precession patterns for 60 mrad cone semiangle (a) and 40 mrad cone semiangle (b). Spiral distortions in the projector lens alters the shape of the spots and shifts their positions, preventing straightforward intensity measurement. Using a smaller cone semiangle gives an improved and easier to measure spot pattern.

the tilt control sensitivity. It is advantageous to operate in the bright mode to make best use of the scan generator's dynamic range. A scan amplitude of 3.5 V yields about 40 mrad in this mode.

Careful alignment of the precession device yields very high quality patterns (the procedure is given in the Appendix). Figure 9(a) is a montage of probe images at several points along the precession route for a near-aligned condition. The probe has been spread to about 50 nm to clearly show the crystal edge. Each tile in the montage contains a different image of the specimen representing a specific tilt condition, and for each scan step the beam becomes slightly displaced from the centered beam in the image plane (not

apparent in the figure). This probe wandering causes delocalization when the beam is precessed at full speed. The center image is the composite of the full precession; the specimen image becomes blurred and the probe becomes delocalized if alignment is poor. Moving the specimen closer to eucentric height and optimizing the lens settings and aberration compensations improves both localization of the probe and sharpness of the specimen features [Fig. 9(b)].

The 2000FX implementation can generate usable patterns using cone semiangles up to about 50 mrad. Appreciable projector distortions result beyond this point [Fig. 10(a)], but patterns may still be measurable if integration methods less sophisticated than autocorrelation are used. The highest quality patterns are obtainable using cone semiangle between 0 and 40 mrad [Fig. 10(b)]; probe localization is excellent up to about 35 mrad, yielding approximate probe size of 25 nm for a very well-aligned experiment. A larger 50 nm probe is readily achievable with about 15 min of alignment time. The instrument has been used to obtain high-quality precession patterns for particle regions as small as 30 nm.

ACKNOWLEDGMENTS

APPENDIX: PRECESSION ALIGNMENT PROCEDURE

Alignment of the precession system is similar to conventional column alignment, e.g., from the top of the column downward. With the column previously aligned for imaging, the subsequent precession alignment described here is straightforward and can typically be completed within about 15 min.

The following conditions are requisite for a high-quality precession experiment:

(1) Specimen on-zone to within 0.5 mrad. Precession patterns are quite tolerant of a slightly off-zone condition, but a better on-zone condition will yield better accuracy in the intensity integration.
(2) Specimen located close to or at eucentric height in the z-direction.
(3) Beam well-aligned with the optic axis (HV centering).
(4) Diffraction spot carefully focused and intermediate lens stigmation corrected.
(5) De-scan coils roughly zeroed to minimize deflector nonlinearity and avoid parallax distortions.
(6) If a CCD camera is used, spot size and convergence set so as to not overexpose the camera.

Highest tilt is achievable when the objective lens system is excited to its optimal current setting: this is the point
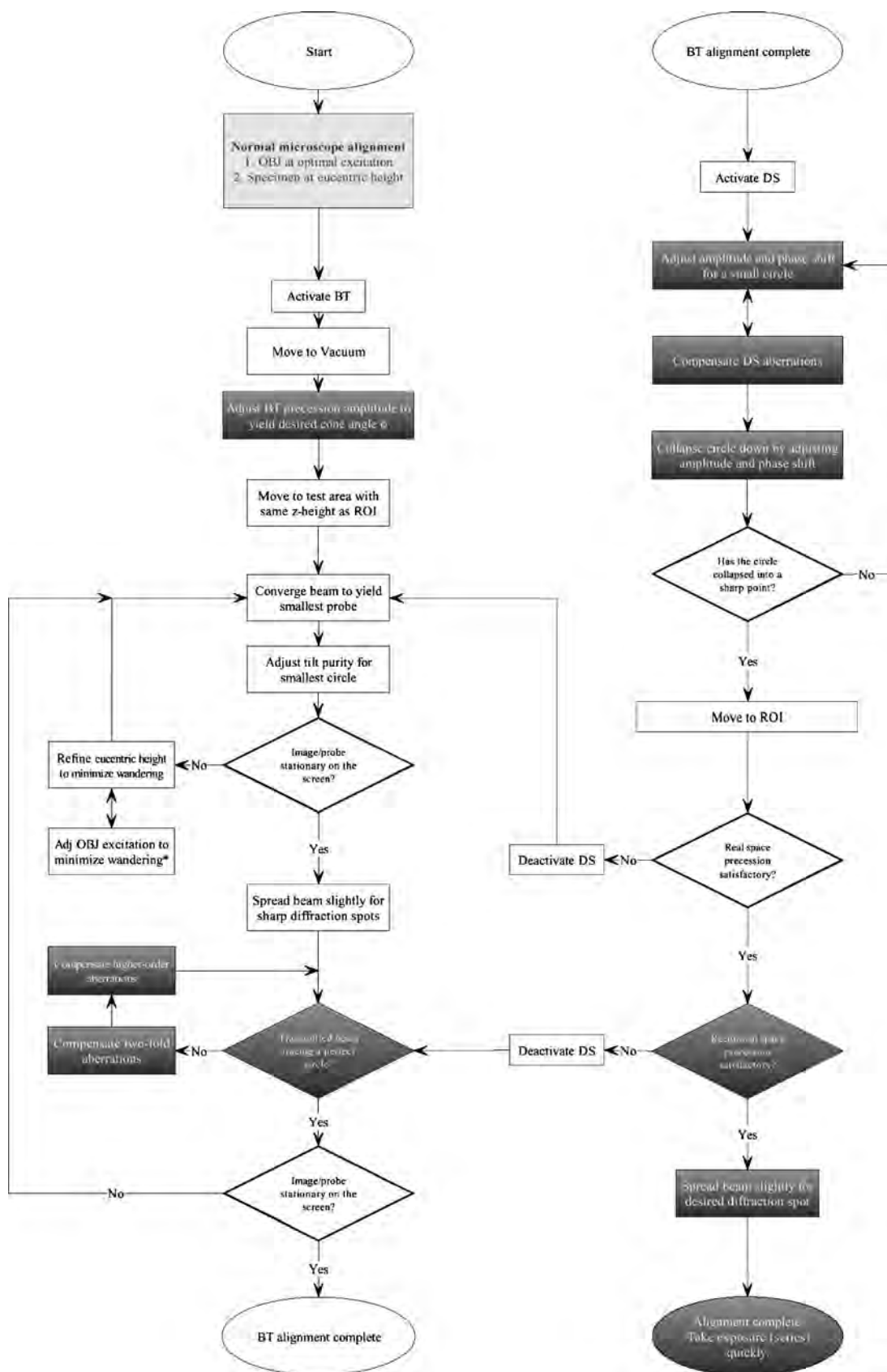
FIG. 11. Precession alignment flow chart. Operations conducted in real space have white background color; reciprocal space operations have black background color.

where lens aberrations are lowest and the probe size smallest. Optimal objective excitation is factory-specified and can be obtained from the microscope manufacturer. Objective excitation is the most important parameter in the precession experiment, and the alignment of the system derives from this starting point.

The procedure for alignment for the NWU-designed systems is detailed pictorially in the flow diagram in Fig. 11. The objective should be optimally excited and the region of interest (ROI) located at optimum focus. After conventional alignment of the imaging system, precession alignment begins by exciting the scan in the upper tilt coils (BT) to the desired cone angle in the diffraction mode. One can determine cone angle by referencing the scan against diffraction spots or a calibration pattern. With scan on, switching to image mode will yield a circle that shows the intersection of the hollow cone with the specimen. The circle may be distorted due to objective aberrations. If the scan rate is lowered to below 1 Hz, one can easily see the beam tracing a path in real space through the aberrations in the lens field.

Shift-tilt purity correction (sometimes also called tilt "wobbler" alignment) should be adjusted next to obtain the smallest and least distorted ring pattern possible. This adjustment aligns the stacked BT deflector coils, compensating rotations and minor dipole nonuniformities. Since the beam is swept around a perimeter inside the tilt coil, the adjustment may not result in the same shift-tilt purity settings as the conventional two-axis tilt purity adjustment, which sweeps only along the two major axes.

Continuing in real space, beam convergence should be readjusted if necessary to obtain minimum probe size. This will generate a fine ring pattern (possibly distorted). If the tilt purity correction forms a fine spot and the specimen image moves minimally with BT scan active, the real space tilt alignment is complete. If not, specimen height must be adjusted to better intersect the convergence point of the cone and subsequent refinement must be carried out. The three variables—objective excitation, sample height, and tilt purity—can be iteratively refined in this way until a reasonably stationary hollow cone probe and sample image are achieved in real space.

The next step is to refine the reciprocal space behavior of the BT precession. It is usually convenient to do this alignment off the specimen in vacuum to make use of a sharp and bright transmitted beam. In the diffraction mode, the scan parameters on the precession control panel can be used to compensate for the aberrations and make the ring round. If digital capture is available, one can use a circle overlay as a reference for applying the compensations until the pattern is incident or concentric with the reference circle. If the real space alignments were done well, the compensations should have little or no effect on the real space behavior of the beam. Otherwise, refinement of real space alignment may be necessary after BT alignment in reciprocal space. If the

scanned circle in diffraction space is concentric and the real space image and probe are stationary, BT alignment is complete.

The de-scan can now be activated. The procedure for DS alignment is easier and less sensitive than the BT. The software for this system has real-time updates, so one can simply "wobble" the slider bars for DS amplitude and phase shift to perturb the de-scanned pattern, revealing the direction the alignment should progress in order to collapse the BT circle down to a sharp spot. Elliptical compensations for twofold distortions can be applied concurrently to form a sharp point. Moving the specimen into the path of the beam allows the user to check the quality of the alignment for higher angle reflections.

Once the alignment of the transmitted beam is complete and a high quality zone axis pattern is obtainable, it is advantageous to double-check real-space alignment before switching to the precession mode to take exposures. The conditions in the microscope are dynamic (specimen drift, lens instability) making it important to take exposures quickly before alignment conditions require readjustment. Along with the diffraction pattern exposures, it is useful to record the precession amplitudes in the form of voltages and record an image of the BT circle (DS disabled) to document the cone semiangle.

[1] P. E. Batson, N. Dellby, and O. L. Krivanek, Nature (London) **418**, 617 (2002).
[2] B. Kabius *et al.*, J. Electron Microsc. **51**, S51 (2002).
[3] L. J. Allen *et al.*, Phys. Rev. Lett. **91**, 105503 (2003).
[4] W. Sinkler, E. Bengu, and L. D. Marks, Acta Crystallogr., Sect. A: Found. Crystallogr. **54**, 591 (1998).
[5] W. Sinkler and L. D. Marks, Ultramicroscopy **75**, 251 (1999).
[6] A. Subramanian and L. D. Marks, Ultramicroscopy **98**, 151 (2004).
[7] R. Vincent and P. A. Midgley, Ultramicroscopy **53**, 271 (1994).
[8] C. S. Own, L. D. Marks, and W. Sinkler, Acta Crystallogr., Sect. A: Found. (submitted).
[9] J. Gjønnes *et al.*, Acta Crystallogr., Sect. A: Found. Crystallogr. **54**, 306 (1998).
[10] K. Gjønnes *et al.*, Acta Crystallogr., Sect. A: Found. Crystallogr. **54**, 102 (1998).
[11] M. Gemmi *et al.*, Acta Crystallogr., Sect. A: Found. Crystallogr. **59**, 117 (2003).
[12] J. Gjønnes, V. Hansen, and A. Kverneland, Microsc. Microanal. **10**, 16 (2004).
[13] C. S. Own, A. Subramanian, and L. D. Marks, Microsc. Microanal. **10**, 96 (2004).
[14] R. Vincent and D. M. Bird, Philos. Mag. A **53**, L35 (1986).
[15] K. Gjønnes, Ultramicroscopy **69**, 1 (1997).
[16] B. S. Berg *et al.*, Ultramicroscopy **74**, 147 (1998).
[17] M. Gemmi, in *Electron Crystallography and Cryo-Electron Microscopy*, edited by J. Puiggali *et al.* (Barcelona Universitat Politecnica de Catalunya, Barcelona, 2001).
[18] S. Franco, *Design with Operational Amplifiers and Analog Integrated Circuits* (McGraw-Hill, New York, 2002).
[19] P. Horowitz and W. Hill, *The Art of Electronics* (Cambridge University Press, New York, 1989).
[20] *Op Amps for Everyone* (TI application note SLOD006B), edited by R. Mancini (Texas Instruments, Dallas, 2002).
[21] *Precession*, Northwestern University, 15 August 2004, ⟨http://www.numis.northwestern.edu/Research/Current/precession.shtml⟩
[22] R. Kilaas, L. D. Marks, and C. S. Own, Ultramicroscopy **102**, 233 (2005).